Translational diffusion of water inside hydrophobic carbon micropores studied by neutron spectroscopy and molecular dynamics simulation

S. O. Diallo, L. Vlcek, E. Mamontov, J. K. Keum, Jihua Chen, J. S. Hayes, Jr., and A. A. Chialvo

Translational Diffusion of Water inside Hydrophobic Carbon Micropores Studied by Neutron Spectroscopy and Molecular Dynamics Simulation

S.O. Diallo,[1, *] L. Vlcek,[2] E. Mamontov,[3] J.K. Keum,[4] Jihua Chen,[5] J.S. Hayes Jr.,[6] and A.A. Chialvo[2, †]

[1]*Quantum Condensed Matter Division, Oak Ridge National Laboratory, Oak Ridge, Tennessee 37831, USA*
[2]*Chemical Sciences Division, Oak Ridge, National Laboratory, Tennessee 37831, USA*
[3]*Chemical and Engineering Science Division, Oak Ridge National Laboratory, Oak Ridge, Tennessee 37831, USA*
[4]*Instrument and Source Division, Oak Ridge National Laboratory, Oak Ridge, Tennessee 37831, USA*
[5]*Center for Nanophase Materials Sciences, Oak Ridge National Laboratory, Oak Ridge, Tennessee 37831, USA*
[6]*American Technical Trading, Incorporated, P.O. Box 273, Pleasantville, New York 10570, USA*

When water molecules are confined to nanoscale spacings, such as in the nanometer size pores of activated carbon fiber (ACF), their freezing point gets suppressed down to very low temperatures (~ 150 K), leading to a metastable liquid state with remarkable physical properties. We have investigated the ambient pressure diffusive dynamics of water in microporous Kynol$^{\mathrm{TM}}$ACF-10 (average pore size $\sim$11.6 Å, with primarily slit-like pores) from temperature $T = 280$ K in its stable liquid state down to $T = 230$ K into the metastable supercooled phase. The observed characteristic relaxation times and diffusion coefficients are found to be respectively higher and lower than those in bulk water, indicating a slowing down of the water mobility with decreasing temperature. The observed temperature-dependent average relaxation time $\langle \tau \rangle$ when compared to previous findings indicate that it is the width of the slit pores - not their curvature - that primarily affects the dynamics of water for pore sizes larger than 10 Å. The experimental observations are compared to complementary molecular dynamics simulations of a model system, in which we studied the diffusion of water within the 11.6 Å gap of two parallel graphene sheets. We find generally a reasonable agreement between the observed and calculated relaxation times at the low momentum transfer Q ($Q \leq 0.9$ Å^{-1}). At high Q however, where localized dynamics becomes relevant, this ideal system does not satisfactorily reproduce the measurements. Consequently, the simulations are compared to the experiments at low Q, where the two can be best reconciled. The best agreement is obtained for the diffusion parameter D associated with the hydrogen-site when a representative stretched exponential function, rather than the standard bi-modal exponential model, is used to parameterize the self-correlation function $I(Q, t)$.

I. INTRODUCTION

Fluids confined to nano-cavities, or restricted to surfaces are pervasive in nature [1]. Such nano-confinement often gives rise to unusual physical properties, that are distinct from those in the bulk liquid [2–4]. In the case of water, nano-confinement suppresses crystallization altogether, modifying the water phase diagram and leading to a metastable supercooled liquid. Nano-porous carbon compounds are perfect examples of confining media that have inspired research on supercooled water [5, 6], and that continue to stimulate applied research for developing for example high-performing membranes for water desalination, nanofluidic devices, and alternative drug delivery methods[7].

The dynamical properties of supercooled water constrained in cylindrical pores have been extensively investigated with neutron scattering using various hydrophilic silica materials such as MCM-14 or FSM-12 [8–13], and some hydrophobic carbon systems such as carbide-derived carbon (CDC)[14], single-wall (SWNT)[15], and double-wall nanotubes (DWNT) [15, 16]. In real physical systems however, water confinement occurs under various spatial and geometrical restrictions. Understanding not only the effects of varying pore size on the structural and dynamical properties of water, but also the influence of different pore shapes is thus of great scientific importance.

The present study aims to understand how supercooled water behaves when it is confined inside a hydrophobic pore structure that is non-cylindrical, and thereby evaluate the effect of geometry on the water dynamics. Specifically, we here examine the characteristic diffusive dynamics of water confined in the narrow pores of Activated Carbon Fiber (ACF-10) using Quasi-Elastic Neutron Scattering (QENS). The observed average characteristic relaxation $\langle \tau \rangle$ and diffusion coefficient D (associated with the hydrogen sites of water) indicate a diffusion that is slower than in the bulk liquid, with an Arrhenius behavior with characteristic energy barriers E_A in the range $14 \leq E_A \leq 29$ kJ/mol, depending on the fit model of various characteristic parameters. Our molecular dynamics simulation of water confined between two parallel flat graphene-surfaces, while not fully representative of the real physical system, shows qualitatively the same systematic trend with temperature, with an $E_A \simeq 19$ kJ/mol. By comparing the present findings with previ-

*Electronic address: `omardiallos@ornl.gov`
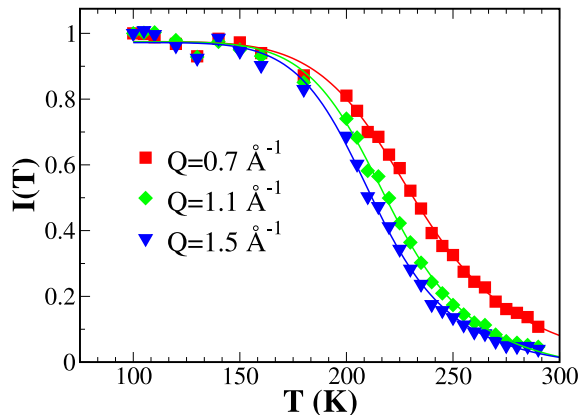†Electronic address: `chialvoaa@ornl.gov`

FIG. 1: (Color online) Temperature dependence of the integrated elastic scattering $I(T)$ of water confined in ACF-10, at a few selected momentum transfers Q. Data are normalized with respect to the lowest temperature ($T_0 = 100$) K, as indicated. The onset of observable diffusive dynamics on BASIS is marked by the departure from a monotonically varying slope in $I(T)$ at low temperatures to a more rapidly changing slope at the higher temperatures. The solid lines are model fits to data, corresponding to an activation energy E_A =14-15 kJ/mol.
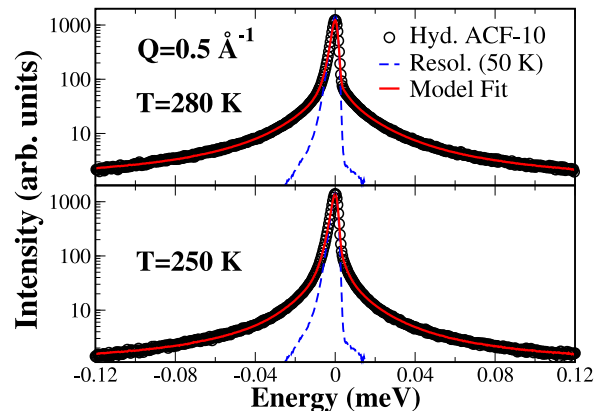

FIG. 2: (Color online) Representative spectrum of water in AFC-10 at $Q = 0.5$ Å^{-1}, as observed on BASIS, plotted with the measured BASIS resolution function at 50 K (blue dashed line). Data at 280 K (top panel) and at 250K (bottom panel) are shown. The open circles represent the total observed signal from the water wetted ACF-10 sample in the Al holder. The red solid lines are model fits to the experimental data, as discussed in the text.

ous experimental observations, we conclude that at any given thermodynamic condition, it is primarily the confining pore dimension, and not its geometry, that dictates the dynamical behavior of confined water. The measured and calculated intrinsic intermediate scattering function $I_{in}(Q,t)$ (or self-correlation function) at ambient conditions could be satisfactorily reconciled at the low momentum transfer Q (≤ 0.9 Å^{-1}), where localized dynamics are not as relevant.

II. NEUTRON EXPERIMENTS

In this section, we describe the ACF-10 sample, and the various steps involved in preparing for the neutron measurements. We also discuss the actual measurements performed on the backscattering spectrometer (BASIS) at Oak Ridge National Laboratory (ORNL), USA [17]. This inverted geometry spectrometer has an excellent energy resolution of 3.5 μeV (2 × Half-Width-at-Half-Maximum = 2 ×Γ_r) at the elastic line, and covers a momentum Q and energy E transfer range, respectively 0.3 $\leq Q \leq 1.9$ Å^{-1}, and -0.12 $\leq E \leq 0.12$ meV when operated with incident neutron beam with wavelength $\lambda_i = 6.4$ Å ($\Delta\lambda_i = \pm 0.5$ Å), corresponding to an energy bandwidth of $1.71 \leq E_i \leq 2.35$ meV.

A. Sample Details

The Kynol$^{\text{TM}*}$ ACF-10 (ACF-1603-10) sample was provided to us by American Technical Trading (ATT), NY. With its human hair-like appearance, this activated carbon fiber is reported to have an 'average' length of 2-4 mm, and diameter ~ 10 μm, which is consistent with our transmission electron microscopy conducted at the Oak Ridge National Laboratory's Center of Nanophase Materials Sciences. Previously reported scanning tunneling microscopy (STM) of ACF-10 [18–20] has revealed a highly sinuous pore network with a predominant and uniform nanometer size pore distribution ($\sim 90\%$ of the total pore volume of ~ 0.4-0.5 cc/g determined from N$_2$ adsorption isotherms [19, 21]). The remainder of the pore volume consists of largely random mesopores and some ultra-micropores. Various other measurements including thermodynamics[18, 22], small-angle neutron and X-ray scattering [23, 24] of ACF-10 have also confirmed the interconnected pore structure of ACF-10, which is made primarily of elongated curvy slit-pores. The pores themselves are just the voids or gaps between distorted (curled or curved, and not necessarily parallel) graphene sheets, much like empty spaces within a dense pile of potato chips, but comparatively smaller [25]. The key here is that the pores in ACF-10 are clearly not of the cylindrical-type as in the carbon or silica nanotubes, but rather of irregular slit-geometry, as evidenced in STM. This different pore structure offers a new platform for investigating fluids in confined geometries, in non-cylindrical shaped pores and evaluate the effect of pore

geometry. For the current ACF-10 sample, the micropore size distribution is $\sim$11.6$\pm$4 Å, as determined from N_2 adsorption isotherms [19, 21] using the Dubnin-Astakhov equation [26]. The nominal sample specific surface area is about 1000 m^2/g, as confirmed at the time of manufacture by iodine number testing, which correlates well with BET calculations in this range [19].

To prepare for the neutron experiments, we outgassed the as-provided ACF-10 sample for 36 hours at 473 K in a vacuum oven to remove all of the bulk-like water, and most of the surface water that was originally present in the as-received sample. We then exposed approximately 2.3 grams of the 'dried' batch to 99.9% humidity in a desiccator for several hours. The hydration level reached after 24 hours was 21%, as determined from the relative weight change of the sample. This rather important hydration level signals the possible presence of hydrophilic groups (oxygenated) in an otherwise totally hydrophobic sample. Since this hydration amount is relative to the ' drying' conditions set above, the diffusive dynamics reported in this work are those of all water molecules present inside the porous carbon network. The neutron being primarily sensitive to hydrogen atoms in QENS measurements, the measurements yield the characteristic relaxations of all confined water molecules. The hydrated sample was thus carefully loaded within a 2 mm gap of two concentric Al cylinders to minimize multiple scattering. The subsequently indium-sealed containers were anchored to the copper finger of a close-cycle refrigerator (CCR) stick which allowed to control the sample temperature between 20 to 500 K, within $\pm$0.02 K.

B. Elastic Incoherent Scattering

We started our neutron measurements with a rapid collection of elastic scattering data of the hydrated ACF sample, on cooling it from room temperature down to $\sim$100 K. The purpose of these scans were two-fold; (1) to investigate the absence of bulk-like water in the samples, and (2) to determine a temperature range where the dynamics can be suitably studied on the spectrometer. Fig. 1 shows the integrated elastic intensity $I(T)$ as a function of temperature for selected Q, normalized to the lowest temperature data collected at 100 K such that $I(T)/I(T_0)$ equals unity. The elastic intensity at each temperature was obtained by integrating the corresponding spectrum around its elastic peak, over a small energy range $\pm 2\Gamma_r$, corresponding to the resolution width. Assuming an isotropic harmonic system, we can expect the elastic intensity to be proportional to $\exp\left[-Q^2\langle r^2(T)\rangle/3\right]$ [27, 28], where $\langle r^2(T)\rangle$ represents the mean square displacement associated with the hydrogen atoms in the water molecules. An increase in $\langle r^2(T)\rangle$ as a function increasing temperature indicates an increase in mobility of the H-sites of water, and so of water itself. As a result, the elastic intensity within the 3.5 μeV energy resolution would effectively increase with decreasing temperature

TABLE I: Activation energy (rounded to the nearest integer) obtained from various sources. Values from fits of Eq. 1 to the $I(T)$ shown in Fig. 1, and from the Arrhenius temperature dependent diffusion coefficients (Slow (2), KWW, MD, and bulk), as determined from Fig. 6 are shown.

Source	$I(T)$	D_2	D_{KWW}	MD	Bulk
E_A (kJ/mol)	15	14	29	22	24

until it reaches a maximum (plateau region at about 150 K). Crystallization, if present, would be observed as an abrupt change in $I(T)$, which is not seen here at any Q. This suggests that the adsorbed water does not solidify and remains mobile down to at least 150 K, consistent with previous studies [29]. It is worth noting however that the temperature range (K) at which the water dynamics were subsequently simulated and measured, was always above the melting point of water [30, 31].

Assuming that the diffusion process responsible for the observed drop in $I(T)$ has a unimodal and continuous diffusion (single Lorentzian), with temperature dependent width $\Gamma(T) \propto \exp(-E_A/RT)$, the normalized $I(T)$ at each Q can be fitted using the following expression [32],

$$I(T) = A_0 + (1 - A_0)\arctan\left(\frac{\Gamma_r}{\Gamma(T)}\right) \qquad (1)$$

where Γ_r is the half-width of the instrument resolution, defined previously, and A_0 a fraction estimate of the observable molecules that do not participate in the diffusion process. Fitted E_A values are displayed in Table I. The solid lines in Fig. 1 represent the fits obtained, and corresponds to $E_A \simeq 14 - 15$ KJ/mol.

C. Quasi-Elastic Scattering (QENS)

Having determined a suitable temperature range for investigating the diffusion of water in ACF-10 on the spectrometer, we collected high statistical quality QENS data at six temperatures: 280, 270, 260, 250, 240 and 230 K for the hydrated ACF-10 sample. The range of relevant momentum transfer for these QENS measurements is 0.5 $\leq Q \leq$1.7 Å^{-1}, ΔQ = 0.2 Å^{-1}. Fig. 2 depicts representative spectra at two temperatures for $Q = 0.5$ Å^{-1}, plotted against a spectrum obtained at 50 K, which is taken as the instrument resolution function. Below, we discuss our analysis of the QENS data, from which we determine valuable parameters such as the diffusion coefficient, and characteristic relaxation time for the water's hydrogen sites, as a function of temperature.

D. Data Analysis

To analyze the experimental QENS data, we fitted it the observed spectra $S(Q, E)$ at each Q and tempera-
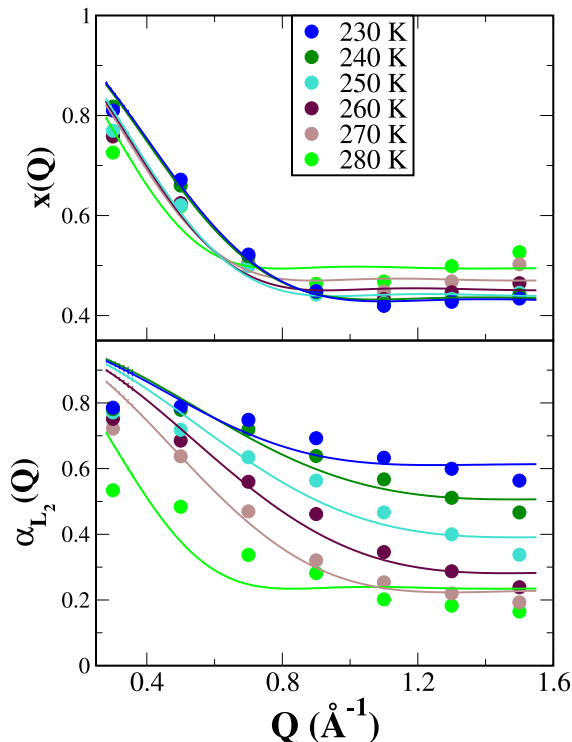
FIG. 3: (Color online) Plot of the fraction of elastic intensity ($x(Q)$ or elastic intensity structure factor ($EISF$)) (top panel) , and the relative weight of the narrowest Lorentzian α_{L_2} (bottom panel) as a function of momentum Q and temperature T. Corresponding temperatures are shown in the legend. Colored solid lines are fits of the generic model for localized dynamics, discussed in the text. The $x(Q)$ parameter is much more sensitive to Q than it is to T, while α_{L_2} reveals a rather strong dependence on Q and T.

ture point to a model function $S_m(Q,E)$ convoluted with the instrument resolution function $R(Q,E)$, plus a linear background term $B(Q,E)$;

$$S(Q,E) = S_m(Q,E) \otimes R(Q,E) + B(Q,E). \quad (2)$$

Within the spectrometer energy window, our model $S_m(Q,E)$ function can be separated into two terms; an elastic part due to 'static' water molecules and a diffusive term $S_d(Q,E)$ coming from the dynamics of the molecules. If we denote the fraction of immobile water molecules by $x(Q)$ (commonly referred to as elastic incoherent structure factor or $EISF$), this model becomes,

$$S_m(Q,E) = x(Q) \times \delta(E) + (1-x(Q)) \times S_d(Q,E) \quad (3)$$

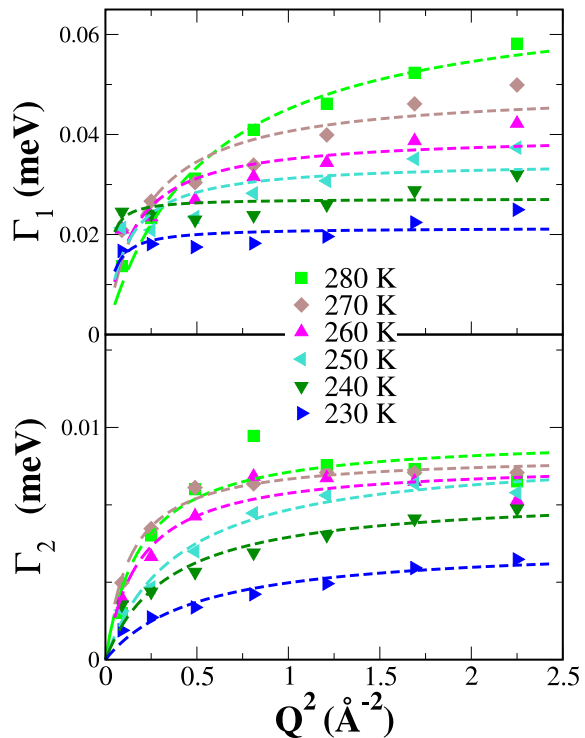where $S_d(E)$ represents the diffusive component of the scattering.

FIG. 4: (Color online) Temperature dependence of the Lorentzian linewidths (Γ_1 and Γ_2) as a function of Q^2. The solid symbols are experimental values, and the dashed lines fits of the jump diffusion model.

III. MOLECULAR DYNAMICS

Here we discuss the methodology employed in our molecular dynamics studies. Computer simulations coupled with QENS provide unparalled insights that are often impossible to obtain with experimental or theoretical approach alone. To further investigate the confinement and temperature effects on the water dynamics using molecular dynamics simulations, we study the time evolution of the intermediate scattering functions (ISF) for the water-hydrogen sites, $I_{in}(Q,t) = \langle \exp(iQ[\mathbf{r}_j(t_0+t) - \mathbf{r}_j(t_0)])\rangle$, where $\mathbf{r}_j(t)$ is the position of the hydrogen-site j at time t, Q is the wavenumber (or momentum transfer), where $\langle \ldots \rangle$ represents the averaging over all j-sites and time origins t_0 [34, 35]. For that purpose we used a pair of flat grapheme plates, $L_x = 28.40$ Å by $L_y = 30.74$ Å , with an inter-plate separation $h = 11.6$ Å. Each graphene plate comprised 364 carbon sites described atomistically as Lennard-Jones spheres characterized by $\epsilon_{cc}/k = 28$ K and $\sigma_{cc}/k = 3.40$ Å [36, 37]. These plates were immersed into an aqueous fluctuating cubic simulation box to perform isobaric-isothermal molecular dynamics at ambient pressure and
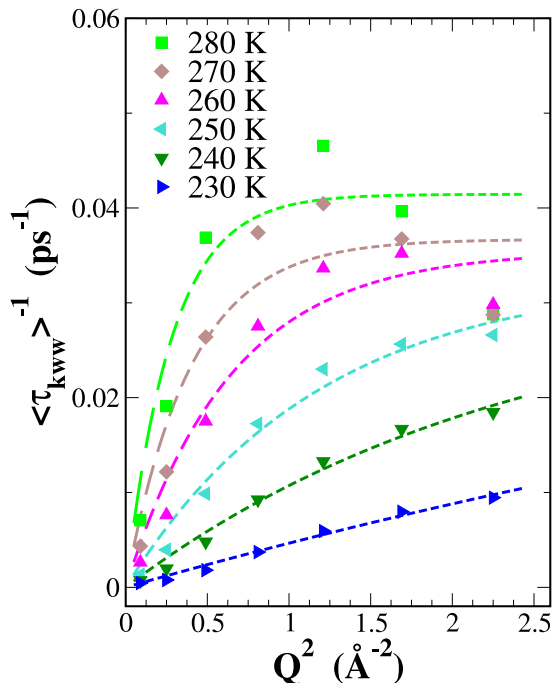
FIG. 5: (Color online) Inverse average relaxation time observed with a KWW model plotted as a function of Q^2 for $230 \leq T \leq 280$ K. The solid symbols are experimental values, and the dashed lines fits of the jump diffusion model.
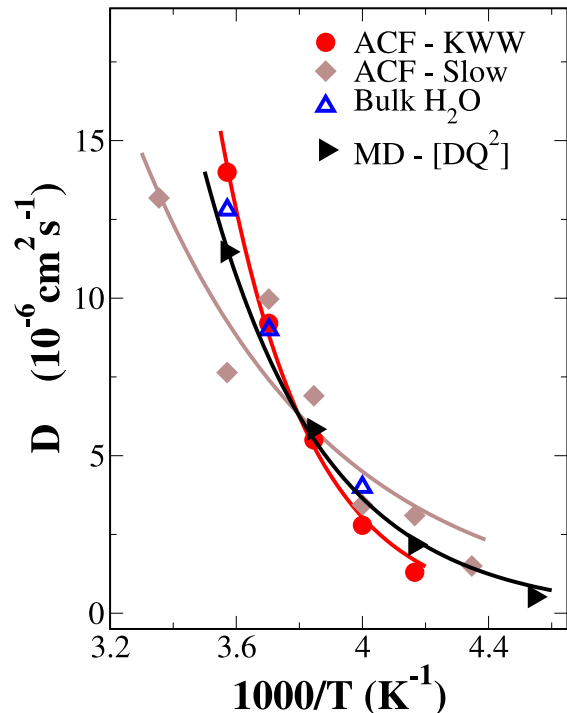

FIG. 6: (Color online) Average diffusion coefficient as a function of $1000/T$. Other reference data are shown for comparison. Dashed lines are fits to an Arrhenius behavior $\sim D_0 e^{-E_a/RT}$

temperatures in the range $220 \leq T \leq 280$ K , according to a Nosé-Poincare symplectic integration algorithm [38, 39] with a time-step of 2.0 fs, where the aqueous environment consists of 2048 SPC/E water molecules [40]. Some useful additional details about the molecular dynamics can be found in the provided supplemental material document.

According to the time-dependent configurational trajectories from simulation we calculated $I_{in}(Q,t)$ at four Q-values, i.e., 1.80, 1.35, 0.90, and 0.45 Å^{-1} corresponding roughly to the intrinsic length-scales characterizing the system, within a time span of about 500 picoseconds. Additional details regarding the simulations are given elsewhere [34, 35]. To characterize the dynamics of confined water and its temperature response we regressed the simulated $I_{in}(Q,t)$ in terms of either a two-exponential function, $\alpha \exp(-t/\tau_1) + (1-\alpha) \exp(-t/\tau_2)$, or a stretched exponential function, $\exp[-(t/\tau_s)^\beta]$, characterized by the relaxation time τ_s and the stretching exponent β.

IV. RESULTS AND DISCUSSION

To accurately represent all diffusive processes of water, the scattering model $S_d(Q, E)$ in Eq. 3 would ideally be a sum of several Lorentzian functions $\sum_i \frac{\Gamma_i}{E^2 + \Gamma_i^2}$, each accounting for a specific diffusion i in the sample. In practice however, QENS data are most reliably characterized by no more than 2 Lorentzians (2L), still providing reasonable representation of all relevant diffusion processes. In general for water, the 2L model works well for an instrument with broad dynamics range such as BASIS, and consists of a fast component, with characteristic width Γ_1, and a slow component with width Γ_2 . The fast component is generally associated with diffusion inside a 'transient' cage (with say radius a_1) made of other water molecules, and the slow component with inter-cage diffusion [41]. In most instances however, whether the 2L is suitable or not, a stretched exponential model (referred to as Kohlrausch-Williams-Watts (KWW) [27, 42] from now on (i.e. $e^{-(t/\tau)^\beta}$ in the time domain or its Fourier-Transform in energy space) can always be used to represent the distribution of proton dynamics present in the sample. We have used both models to fit the data - not
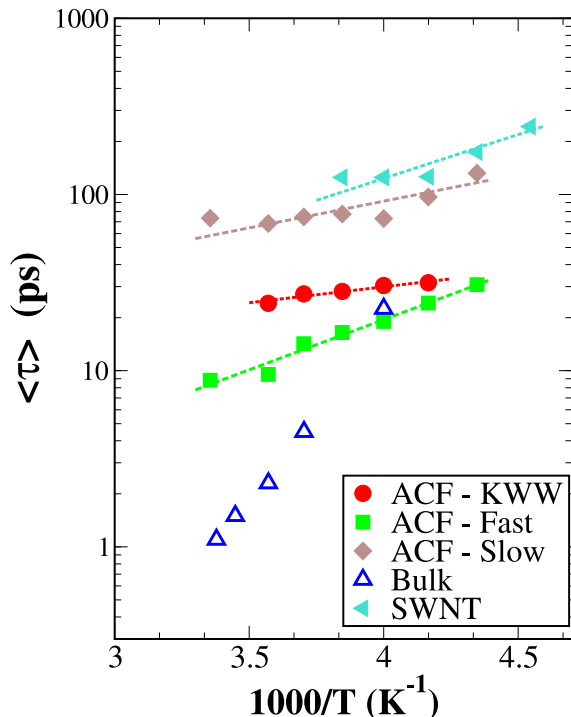
FIG. 7: (Color online) Average relaxation time of water confined in ACF-10 as a function of $1000/T$. Data for bulk water [11, 33], and for water confined in single-wall carbon nanotubes (SWNT)[15] are shown for comparison. The molecular dynamics simulation (MD) results at 0.45 Å^{-1} fitted with the corresponding KWW model are also shown. Dashed lines are fits to an Arrhenius temperature dependence. For meaningful comparison with the SWNT, the ACF values are those obtained using the same jump model in Ref. 15. Eq. 5 applied to both data leads to somewhat lower values but similar temperature dependence.

only for quantifying the dynamics, but also for determining the best model for our particular system. We kept the stretching exponent β fixed to 0.5 at all temperatures for convenience. Our goal was to systematically compare the average relaxation time and diffusion coefficient based on the two models. The other important aim was to compare the experimentally determined characteristic parameters with those obtained in previous experiments with single-wall nanotubes (SWNT), and from molecular dynamics simulations to which we return below. Interestingly, we find that the KWW model yields a better agreement between the simulated and measured diffusion coefficients D, despite the fact that both models are able to reliably capture the experimentally observed values. The relative poor performance of the 2L model fits highlights the fact that proton dynamics in water confined in porous carbon fibers cannot be fully interpreted as a simple mixture of

TABLE II: Temperature dependence of the confining radius (in Å) determined from model fit to the elastic parameter $x(Q)$, and the weight fraction of the second Lorentzian α_{L_2}.

T (K)	280	270	260	250	240	230
a_0(Å)	5.64	4.97	4.75	4.70	4.80	4.10
a_1 (Å)	5.44	3.36	3.08	3.03	3.02	3.59

two relaxation processes. This observation does not exclude the possible existence of two diffusive components with overlapping characteristic times.

In the 2L model, D could only be determined from the slower diffusive component, as generally found in confined systems [43]. We could not extract D for the broad component because Γ_1 does not go to zero at low Q, as is expected in confined diffusion. Assuming a 2L model with Lorentzian components $L_1(Q,E)$ and $L_2(Q,E)$, $S_d(Q,E)$ can be written as,

$$S_d(Q,E) = (1 - \alpha_{L_2}(Q))L_1(Q,E) + \alpha_{L_2}(Q)L_2(Q,E) \tag{4}$$

where $\alpha_{L_2}(Q)$ is the relative weight of the narrow Lorentzian $L_2(Q,E)$. The Q-dependence of this parameter and that of the $x(Q)$ in Eq. 3, which are displayed in Fig. 3, can provide important details regarding the spatial extent of the confined diffusion in the ACF-10 sample. We find an $x(Q)$ that varies little with temperature T but noticeably with momentum transfer Q. In contrast, the parameter $\alpha_{L_2}(Q)$ reveals a rather strong systematic dependence on both Q and T. This allows to estimate the corresponding confining radius a_1 associated with the transient dynamical restriction by fitting α_{L_2} to a generic localized $EISF$ model $\left[f + (1-f)\left(\frac{3j_1(Qa_i)}{Qa_i}\right)^2 \right]$ [44]. The corresponding fits are indicated by the solid lines in Fig. 3 for both $\alpha_{L_2}(Q)$ and $x(Q)$. In the case of $x(Q)$, the radius a_0 extracted yields the spatial confinement due to the nanopores in ACF-10, which is not expected to vary significantly with temperature, as observed here. The fitted values are summarized in Table II. Within a satisfactory fit uncertainty of 10 to 15% (~ 0.3-0.7 Å), we find a clear systematic reduction of the transient confining radius a_1 with decreasing temperature, while f increases.

Using Eq. 4, we have determined the Q-dependence of both Γ_1, and Γ_2, as summarized in Fig. 4. The colored dashed lines are the best model fits using the jump diffusion model,

$$\Gamma_i = \frac{D_i Q^2}{1 + D\tau_{0i} Q^2} \tag{5}$$

where τ_{0i} is the average residence time between jumps, and D_i denotes the diffusion coefficient of process i. From these fits, we could reliably determine the characteristic relaxations for both processes, and the diffusion coefficient D_2 for the slower component. The convergence of
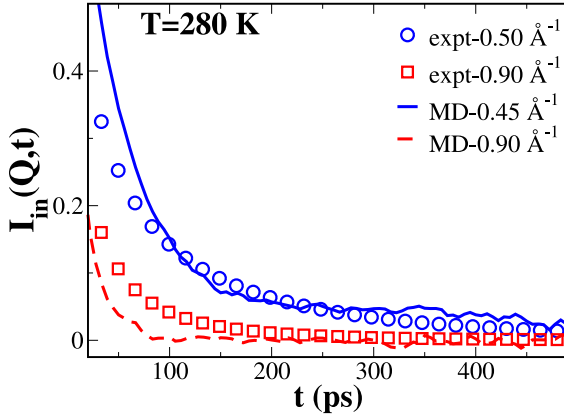
FIG. 8: (Color online) Simulated and calculated intrinsic intermediate scattering function $I_{in}(Q,t)$ of the confined water molecules at 280 K, and selected momentum transfer Q. The measured decay component is $I_{in}(Q,t) = e^{-(t/\tau_{KWW})^\beta}$ where τ_{KWW} and β are the best fit parameters to the experimental data using Eq. 3 with the KWW model.

FIG. 9: (Color online) Comparison of the simulated and measured $\langle\tau\rangle^{-1}$ at low Q. The average relaxation times shown were derived from the KWW model for consistency. The dashed lines are quadratic Q^2 fits to the simulated data.

Γ_1 to a plateau-like regime at low Q complicates the determination of D_1.

We have also evaluated the diffusion characteristics with the alternative KWW model discussed above. The extracted average relaxation times are plotted as a function of Q^2 are shown in Fig. 5. The dashed lines are fitted line using Eq. 5. The fits however reveal different behavior. Specifically, the KWW fits indicate a diffusion process that goes from a jump-type diffusion at ambient temperature to a continuous one below 250 K. For this reason, we only compare the average relaxation time $\langle\tau_{KWW}\rangle$ with those obtained using the 2L model for T between 250 K and 280 K. The extracted diffusion coefficients (D_{KWW} and D_2) and average relaxation time $\langle\tau\rangle$ on the other hand are compared at all temperatures. These comparison are summarized in Figs. 6 and 7. Data from bulk water [11, 33] and SWNT [15] are displayed for comparison, as well as the results from our molecular dynamics at low Q. While the observed KWW diffusion parameter D_{KWW} is a bit smaller than that reported for bulk water, the D_2 or slow diffusion coefficient for the narrow Lorentzian in the 2L model, is significantly smaller. This is not unreasonable since the slow process may be overshadowed in the KWW model by other faster processes. However, we find a much better agreement between the calculated and simulated D with the KWW model, as evidenced in Fig. 6.

Since a direct comparison between the simulated Q-dependent $\langle\tau_Q\rangle$ and the experimentally observed Q-independent $\langle\tau\rangle$ (high Q-limit of the measured $\langle\tau_Q\rangle$ modeled with the jump diffusion model in Eq. 5) is not meaningful, the Q-dependent MD data are not shown in Fig. 7. Instead, we chose to directly compare the sim-
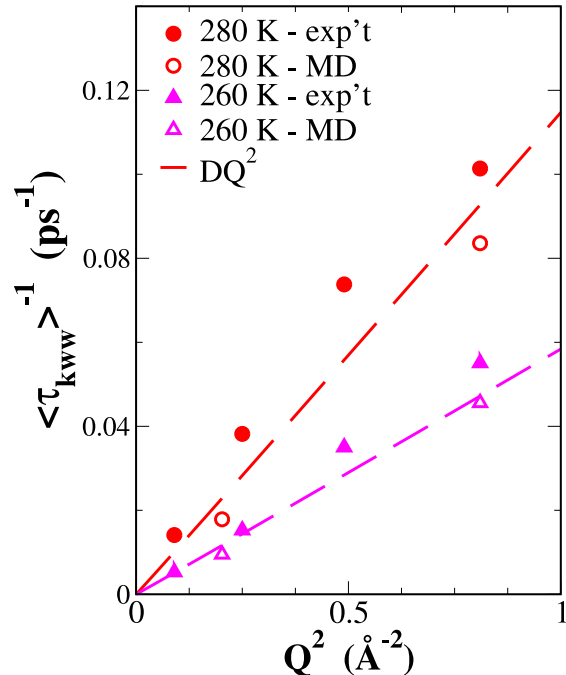
ulated and measured $I(Q,t)$ and the corresponding Q-dependent $\langle\tau_Q\rangle$ at each temperature. To do this, we note that the simulations provide the intrinsic water dynamics while the neutron data contains both the dynamics and structure component. In order to adequately compare the intrinsic intermediate scattering function $I_{in}(Q,t)$, we show in Fig. 8 the simulated $I(Q,t)$ along with only the experimentally observed stretched decay component at 280 K (i.e. $e^{-(t/\tau_{KWW})^\beta}$ where τ_{KWW} is the fitted experimental value – omitting the $EISF$ term). Reasonable agreement can be found between the two, particularly at the lowest Q value. We find some discrepancies in the faster decay at low times which would require further investigations. The long times show generally a reasonable agreement at these low Q values, which unfortunately degrades as Q increases. To highlight the level of agreement at low Q (≤ 1.0 Å^{-1}), we compare the simulated and experimentally observed $\langle\tau_{KWW}\rangle^{-1}$ in Fig. 9. The dashed lines are the corresponding DQ^2 fits from which the D values from molecular dynamics (MD) (shown Fig. 6) were determined.
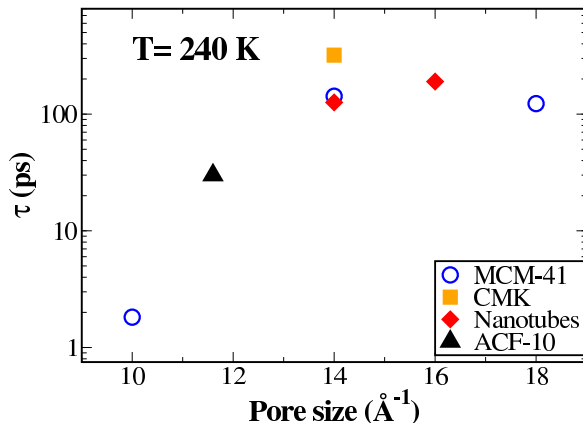
FIG. 10: (Color online) Average relaxation time $\langle\tau\rangle$ of water confined in various microporous materials as a function of confining pore size at selected temperature of 240 K. The open symbols denote values observed for the hydrophilic silica-based (MCM-41S) materials in Ref. [10], and the filled symbols are for hydrophobic carbon-based materials, respectively highly ordered cabon molecular sieves CMK [12], cylindrical carbon nanotubes [15], and our current activated carbon ACF-10 fibers.

V.   CONCLUSIONS

In summary, we have investigated the diffusion of water confined in a network of narrow wavy slits in activated carbon fiber by means of quasi-elastic neutron, and molecular dynamics. By comparing the experimentally observed characteristic diffusion coefficients and relaxation times using the same analysis approach, we conclude that the diffusion of water in ACF-10 is slower than in bulk water but of comparable magnitude to that in cylindrical carbon SWNT (only marginally smaller) and other confining porous media of comparable pore size. Our main conclusion is that above 1 nm, it is not the geometry of the confining pores, but rather their dimensions that primarily affect the dynamics of confined water above 1 nm. Stated differently, the diffusive dynamics of water in pores of the same size above 10 Å, irrespective of whether they are cylindrical or not (slit or not) appears to be of the same order of magnitude for the temperature range investigated, as is illustrated for example in Fig. 10 for temperature T =240 K. Data at other temperatures revealed similar behavior. To validate (or disprove) this perhaps fortuitous observation and evaluate its implication, future experimental work should systematically compare the effect of pore size on

water dynamics in the complete series of ACF made from the same percursor (ACF-15, ACF-20 and ACF-25), to that of comparable hydrophilic silica samples (MCM-41 or other), all modeled using the same approach, since $\langle\tau\rangle$ values are known to be model-dependent. We expect however that MD simulations of water in hydrophobic and hydrophilic pores of varying pore size and geometry would yield predictive behavior. A previous experimental report [14] in which $\langle\tau\rangle$ values obtained from various samples using different models (KWW or 2L) were compared, found no particular dependency of $\langle\tau\rangle$ on pore size.

The experimentally observed relaxation dynamics of confined water are supported by molecular dynamics simulations of an ideal scenario in which water is restricted to diffuse within the interstitial gap between two parallel graphene layers while in equilibrium with its aqueous bulk. The simulations yield a reasonable agreement at low momentum transfer Q ($Q \leq 1.0$ Å^{-1}). The origin of the discrepancies at larger Q remains to be clarified but could arise from either the relatively simple model used, the importance of localized dynamics or rotational motions, the presence of oxygen-containing groups on the graphene surface or edge (carbonyl or hydroxyl for example). Localized dynamics are strongly influenced by surface effects such as surface roughness [35], disorder and corrugation, which becomes dominant at high Q. The simulations yield however a diffusion coefficient D that is in excellent agreement with the experimental value. The comparison between QENS and simulation suggests the need for the additional interrogation of the effect of confined morphology, such as corrugation and pore connectivity, in order to aid the interpretation of the observed discrepancies in the relaxation times.

[1] H.E. Stanley. Mysteries of Water. In M.-C. Bellissent-Funel, editor, *NATO Science Series A*, volume 305. IOS

Press, Amsterdam, 1999.

[2] M. F. Chaplin. Structuring and behaviour of water in

nanochannels and confined. In L.J. Dunne and G. Manos, editors, *Adsorption and Phase Behavior in Nanochannels and Nanotubes*, pages 241–255. Springer, 2009.

[3] Malgorzata Sliwinska-Bartkowiak, Henryk Drozdowski, Mateusz Kempinski, Monika Jazdzewska, Yun Long, Jeremy C. Palmer, and Keith E. Gubbins. Structural analysis of water and carbon tetrachloride adsorbed in activated carbon fibres. *Phys. Chem. Chem. Phys.*, 14:7145, 2012.

[4] C. Alba-Simionesco and B. Coasne and G. Dosseh and G. Dudziak and K.E. Gubbins and R. Radhakrishnan and M. Sliwinska-Bartkowiak. Effects of confinement on freezing and melting. *J. Phys. Condens. Mat.*, 18(6):R15, 2006.

[5] Yang Zhang, Kao-Hsiang Liu, Marco Lagi, Dazhi Liu, Kenneth C Littrell, Chung-Yuan Mou, and Sow-Hsin Chen. Absence of the density minimum of supercooled water in hydrophobic confinement. *J. Phys. Chem. B*, 113(13):5007, 2009.

[6] A. I. Kolesnikov, J.M. Zanotti, C-K. Loong, P. Thiyagarajan, A. P. Moravsky, R. O. Loutfy, and C. J. Burnham. Anomalously soft dynamics ofwater in a nanotube: A revelation of nanoscale confinement. *Phys. Rev. Lett.*, 93(3):035503, 2004.

[7] Alberto Striolo. Water self-diffusion through narrow oxygenated carbon nanotubes. *Nanotechnology*, 18(47):475704, 2007.

[8] A. Faraone, L. Liu, C-Y. Mou, C-W. Yen, and S.-H. Chen. Dynamic Transition in Deeply Supercooled Water Confined in Nanoporous MCM-41-S. *J. Chem. Phys.*, 121:10843, 2004.

[9] S.-H. Chen, L. Liu, E. Frantini, A. Faraone, and E. Mamontov. Observation of fragile-to-strong dynamic crossover in protein hydration water. *Proc. Nat. Acad. Sci. U.S.A.*, 103:9012–9016, 2006.

[10] L. Liu, S-H. Chen, A. Faraone, C-W. Yen, C-Y. Mou, A.I. Kolesnikov, E. Mamontov, and J. Leao. Quasielastic and inelastic neutron scattering investigation of fragile-to-strong crossover in deeply supercooled water confined in nanoporous silica matrices. *J. Phys. Condens. Mat.*, 18:S2261–S2284, 2006.

[11] Shuichi Takahara, Naoya Sumiyama, Shigeharu Kittaka, Toshio Yamaguchi, and Marie-Claire Bellissent-Funel. Neutron scattering study on dynamics of water molecules in mcm-41. 2. determination of translational diffusion coefficient. *J. Phys. Chem. B*, 109(22):1123, 2005.

[12] X.-Q. Chu, K.-H. Liu, M. Tyagi, C.-Y. Mou, and S-H. Chen. Low-temperature dynamics of water confined in a hydrophobic mesoporous material. *Phys. Rev. E*, 82:020501(R), Aug 2010.

[13] S. O. Diallo, E. Mamontov, W. Nobuo, S. Inagaki, and Y. Fukushima. Enhanced translational diffusion of confined water under electric field. *Phys. Rev. E*, 86:021506, 2012.

[14] S. M. Chathoth, E. Mamontov, A. I. Kolesnikov, Y. Gogotsi, and D. J. Wesolowski. Quasielastic neutron scattering study of water confined in carbon nanopores. *Europhys. Lett.*, 95(5):56001, 2011.

[15] E. Mamontov, C.J. Burnham, S-H. Chen, A.P. Moravsky, C-K. Loong, N.R. de Souza, and A.I. Kolesnikov. Dynamics of water confined in single- and double-wall carbon nanotubes. *J. Chem. Phys.*, 124(19):194703, 2006.

[16] X.-Q. Chu, A. I. Kolesnikov, A. P. Moravsky, V. Garcia-Sakai, and S.-H. Chen. Observation of a dynamic crossover in water confined in double-wall carbon nanotubes. *Phys. Rev. E*, 76:021505, 2007.

[17] Eugene Mamontov and Kenneth W. Herwig. A time-of-flight backscattering spectrometer at the spallation neutron source, basis. *Rev. Sci. Inst.*, 82:085109, 2011.

[18] K. Kaneko, C. Ishii, M. Ruike, and H. Kuwabara. Origin of superhigh surface area and microcrystalline graphitic structures of activated carbons. *Carbon*, 30(7):1075, 1992.

[19] M.A. Daley, D. Tandon, J. Economy, and E.J. Hippo. Elucidating the porous structure of activated carbon fibers using direct and indirect methods. *Carbon*, 34(10):1191, 1996.

[20] J. I. Paredes, J. I. A. Martínez-Alonso, and J.M.D. Tascón. Characterization of microporosity and mesoporosity in carbonaceous materials by scanning tunneling microscopy. *Langmuir*, 17(2):474, 2001.

[21] W. Liu and S. Adanur. Desulfurization properties of activated carbons fibers. *J. Eng. Fiber. Fabr.*, 9:70, 2014.

[22] K. Kaneko, K. Shimizu, and T. Suzuki. Intrapore field-dependent micropore filling of supercritical n2 in slit-shaped micropores. *J. Chem. Phys.*, 97(11):8705, 1992.

[23] Takaomi Suzuki, Kasuh Takahiro, and Katsumi Kaneko. The structural change of graphitization-controlled microporous carbon upon adsorption of {H2O} and {N2}. *Chem. Phys. Lett.*, 191(6):569 – 573, 1992.

[24] John D.F. Ramsay. Surface and pore structure characterisation by neutron scattering techniques. *Adv. Colloic Interface Sci.*, 76-77:13, 1998.

[25] J.S. Hayes Jr. Novoloid fibers. *Reprinted from Kirk-Othmer: Encyclopedia of Chemical Technology*, 16:125, 1981.

[26] M. M. Dubinin. Fundamentals of the theory of adsorption in micropores of carbon adsorbents: Characteristics of their adsorption properties and microporous structures. *Carbon*, 27:457, 1989.

[27] S.-H. Chen, C. Liao, F. Sciortino, and P. Gallo, and P. Tartaglia. Model for single-particle dynamics in supercooled water. *Phys. Rev. E*, 59:6708, 1999.

[28] S. Magazú, G. Maisano, F. Migliardo, and A. Benedetto. Mean square displacement evaluation by elastic neutron scattering self-distribution function. *Phys. Rev. E*, 77:061802, Jun 2008.

[29] F. G. Alabarse, J. Haines, O. Cambon, C. Levelut, D. Bourgogne, A. Haidoux, D. Granier, and B. Coasne. Freezing of water confined at the nanoscale. *Phys. Rev. Lett.*, 109:035701, 2012.

[30] C. Vega, E. Sanz, and J. L. F. Abascal. The melting temperature of the most common models of water. *J. Chem. Phys.*, 122(11), 2005.

[31] Shigeharu Kittaka, Shinji Ishimaru, Miki Kuranishi, Tomoko Matsuda, and Toshio Yamaguchi. Enthalpy and interfacial free energy changes of water capillary condensed in mesoporous silica, mcm-41 and sba-15. *Phys. Chem. Chem. Phys.*, 8:3223, 2006.

[32] T. Springer. Topcis in Current Physics. In S.W. Lovesey, and T. Springer, editor, *Dynamics of Solids and Liquids By Neutron Scattering*, volume 3. Springer, Berlin, 1977.

[33] J. Teixeira, M. C. Bellissent-Funel, S. H. Chen, and A. J. Dianoux. Experimental Determination of the Nature of Diffusive Motions of Water-Molecules. *Phys. Rev. A*, 31:1913, 1985.

[34] A. A. Chialvo, L. Vlcek, and P. T. Cummings. Surface corrugation effects on the water-graphene interfacial and

confinement behavior. *J. Phys. Chem. C*, 117(45):23875–23886, 2013.

[35] A. A. Chialvo, L. Vlcek, and P. T. Cummings. Surface strain effects on the watergraphene interfacial and confinement behavior. *J. Phys. Chem. C*, 118(34):19701–19711, 2014.

[36] W.A. Steele. Physical Interaction of Gases with Crystalline Solids .1. Gas-Solid Energies and Properties of Isolated Adsorbed Atoms. *Surface Science*, 36:317–352, 1973.

[37] A. Striolo, K. E. Gubbins, A. A. Chialvo, and P. T. Cummings. Simulated water adsorption isotherms in carbon nanopores. *Mol. Phys.*, 102:243–251, 2004.

[38] Shuichi Nosé. An Improved Symplectic Integrator for Nosé-Poincaré Thermostat. *J. Phys. Soc. Jpn.*, 70(1):75–77, 2001.

[39] H. Okumura, S. G. Itoh, and Y. Okamoto. Explicit symplectic integrators of molecular dynamics algorithms for rigid-body molecules in the canonical, isobaric-isothermal, and related ensembles. *J. Chem. Phys.*, 126(8):084103, February 2007.

[40] H. J. C. Berendsen, J. R. Grigera, and T. P. Straatsma. The missing term in effective pair potentials. *J. Phys. C: Solid State*, 91(24):6269–6271, 1987.

[41] J. Qvist, H. Schober, and B. Halle. Structural dynamics of supercooled water from quasielastic neutron scattering and molecular simulations. *J. Chem. Phys.*, 134:144508, 2011.

[42] H. Li, E. Fratini, W-S. Chiang, P. Baglioni, E. Mamontov, and S-H. Chen. Dynamic behavior of hydration water in calcium-silicate-hydrate gel: A quasielastic neutron scattering spectroscopy investigation. *Phys. Rev. E*, 86:061505, Dec 2012.

[43] J. M. Zanotti, M-C. Bellissent-Funel, and S-H. Chen. Relaxational dynamics of supercooled water in porous glass. *Phys. Rev. E*, 59:3084, 1999.

[44] J. M. Zanotti, M-C. Bellissent-Funel, and J. Parello. Hydration-Coupled Dynamics in Proteins Studied by Neutron Scattering and NMR: The Case of the Typical EF-Hand Calcium-Binding Parvalbumin. *Biophys. J.*, 76:2390, 1999.

See Supplemental Material (SM) at [   ] for additional details regarding the simulations.